Cooling dynamics of energized naphthalene and azulene radical cations

Jason W. L. Lee,[1] Mark H. Stockett,[2] Eleanor K. Ashworth,[3] José E. Navarro Navarrete,[2] Eva Gougoula,[1] Diksha Garg,[1] MingChao Ji,[2] Boxing Zhu,[2] Suvasthika Indrajith,[2] Henning Zettergren,[2] Henning T. Schmidt,[2] and James N. Bull[3, a)]

[1)] *Deutsches Elektronen-Synchrotron DESY, Notkestr. 85, 22607 Hamburg, Germany*

[2)] *Department of Physics, Stockholm University, SE-10691 Stockholm, Sweden*

[3)] *School of Chemistry, Norwich Research Park, University of East Anglia, Norwich NR4 7TJ, United Kingdom*

Naphthalene and azulene are isomeric polycyclic aromatic hydrocarbons and are topical in the context of astrochemistry due to the recent discovery of substituted naphthalenes in the Taurus Molecular Cloud-1 (TMC-1). Here, the thermal- and photo-induced isomerization, dissociation, and radiative cooling dynamics of energized (vibrationally hot) naphthalene (Np^+) and azulene (Az^+) radical cations, occurring over the microsecond to seconds timescale, are investigated using a cryogenic electrostatic ion storage ring, affording 'molecular cloud in a box' conditions. Measurement of the cooling dynamics and kinetic energy release distributions for neutrals formed through dissociation, until several seconds after hot ion formation, are consistent with establishment of a rapid (sub-microsecond) $Np^+ \rightleftharpoons Az^+$ quasi-equilibrium. Consequently, dissociation by C_2H_2-elimination proceeds predominantly through common Az^+ decomposition pathways. Simulation of the isomerization, dissociation, recurrent fluorescence, and infrared cooling dynamics using a coupled master equation combined with high-level potential energy surface calculations (CCSD(T)/cc-pVTZ), reproduce the trends in the measurements. The data show that radiative cooling *via* recurrent fluorescence, predominately through the Np^+ $D_0 \leftarrow D_2$ transition, efficiently quenches dissociation for vibrational energies up to ≈1 eV above dissociation thresholds. Our measurements support the suggestion that small cations, such as naphthalene, may be more abundant in space than previously thought. The strategy presented in this work could be extended to fingerprint the cooling dynamics of other PAH ions for which isomerization is predicted to precede dissociation.

I. INTRODUCTION

Naphthalene and azulene (FIG. 1) are the simplest polycyclic aromatic hydrocarbon (PAH) isomers and are the archetypal couple for PAH isomerization dynamics. PAHs are commonly generated in flames and incomplete combustion of organic material,[1,2] and are surmised to be ubiquitous in space.[3,4] Notably, 10–20% of interstellar carbon is thought to exist as PAHs,[5,6] and are conjectured to be major contributors to IR emissions in astronomical observations, including the so-called unidentified infrared emission (UIE) bands[5,7] and the aromatic infrared bands (AIBs) in UV-irradiated astrochemical environments.[8–10] In the context of interstellar PAHs, naphthalene and derivatives are highly topical following the discovery of two isomers of cyanonaphthalene in Taurus Molecular Cloud-1 (TMC-1) through assignment of rotational lines, with an abundance six orders of magnitude higher than standard modeling predicts.[11] This discovery has, at long last, identified specific PAHs in space. Prior to this discovery, it was thought that PAHs with less than ca. 50 atoms would not radiatively stabilize following ionizing interactions;[12–14] clearly these models need revision and quantitative laboratory data for calibration.[15] Shortly after the discovery of the cyanonaphthalenes, the indene and 2-cyanoindene molecules were identified using similar methodology and, again, found to be several orders of magnitude more abundant than modeling predicted.[16,17] In addition to neutral PAHs, charged forms are thought to control the ionization balance in molecular clouds,[18] influence protoplanetary ion-molecule chemistry, and the neutrals are important sources of photoelectrons in the diffuse interstellar medium and in the surface layers of protoplanetary disks.[19–21]

Following the first report of the thermal rearrangement of (neutral) azulene to naphthalene in 1947,[22] there have been numerous experimental studies on their light- and heat-induced interconversion – see Wentrup and co-workers[23] for a recent summary. Experiments on the radical cations of naphthalene (Np^+) and azulene (Az^+), and related PAH cations, have concluded that photoexcitation is followed by rapid internal conversion (picoseconds) to recover the ground electronic state.[24–27] Significantly, for Np^+ and Az^+, because iso-

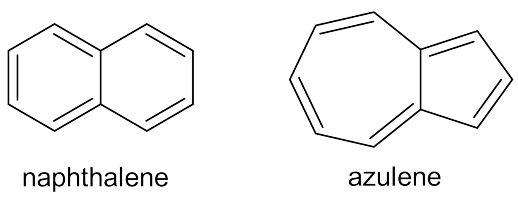

FIG. 1. Molecular structures of the $C_{10}H_8$ isomers naphthalene and azulene. The radical cations are denoted Np^+ and Az^+, respectively.

[a)] Electronic mail: james.bull@uea.ac.uk

merization barriers are lower than dissociation barriers, isomerization reaction rates are higher and, therefore, energized Az^+ or Np^+ may (over certain internal energy windows) statistically dissociate *via* common intermediates and mechanisms.[24,28–33] These dynamics have been partially confirmed through calculation of potential energy surfaces and kinetic modeling of the isomerization and dissociation pathways,[34–37] although clear experimental characterizations are lacking.

The cooling dynamics of energized PAH ions occurring over extended timescales (e.g., microseconds to milliseconds) can be probed using ion storage devices, such as the approach implemented by Bernard et al.,[38] in which the slow thermal decay of activated Np^+ was studied in a room-temperature electrostatic ion storage ring. The study highlighted the importance of both infrared (IR) radiative cooling, occurring through vibrational transitions,[39] and recurrent fluorescence (RF), with the latter corresponding to photon emission from thermally-populated electronic states *via* inverse internal conversion.[40,41] A subsequent work by Saito et al.[42] directly observed RF for the $D_0 \leftarrow D_2$ transition in energized Np^+. While room temperature storage ring experiments can access 'slow' dynamics, occurring up to milliseconds after ion formation, they cannot unequivocally probe the 'ultraslow' processes occurring over milliseconds and up to seconds. In order to investigate these latter processes, the Double ElectroStatic Ion Ring ExpEriment (DESIREE) at Stockholm University has been utilized in single ring experiments.[43] For example, some of the present authors studied 1-cyanonaphthalene radical cations (1-CNN^+) at DESIREE to infer the importance of RF in the cooling dynamics relevant in astrochemical environments,[15,44] and, as a result, proposed that RF-assisted cooling of PAHs may be more common than previously thought. A key advantage of DESIREE is access to these ultraslow timescales due to the cryogenic and ultra-high vacuum conditions. It is also worth noting that molecular isomerization in ion storage experiments is often difficult to fingerprint.[45,46]

Due to the importance of naphthalene and azulene as fundamental PAH isomers and because of their relevance in astrochemistry as precursors in 'bottom-up' growth mechanisms for larger PAHs,[47] the present report seeks to: (i) measure cooling rates for energized Np^+ and Az^+ under 'molecular cloud in a box' conditions,[48,49] (ii) provide an assessment of the isomerization between Np^+ and Az^+, based on measuring kinetic energy release (KER) distributions associated with dissociation and monitoring time-dependent cooling dynamics following thermal- and photo-activation, and (iii) assess the importance of RF in the cooling dynamics of Np^+ and Az^+, helping to imply the preponderance of these species in space. Furthermore, the present experiments are the first on the vibrationally-hot naphthalene-azulene cation couple conducted under conditions mimicking the low-temperature (T =10–20 K), collision-free environment found in molecular clouds. Such hot ions may be generated in space following the absorption of UV radiation and internal conversion to recover the ground electronic state. We chose to study the radical cations of the precursor naphthalene and azulene molecules rather than dehydrogenated species because they are the most astrochemically relevant and because of additional isomer complications with the dehydrogenated forms.

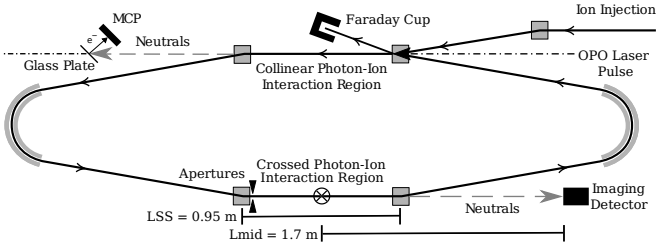

FIG. 2. Schematic diagram of the ion storage ring in DESIREE at Stockholm University used in this study. Cryogenic cooling of the ring to $T \approx 13$ K gives a residual gas density of $\approx 10^4$ particles/cm^3 (mostly H_2).[50] Neutral products formed in the either straight section are not confined by the electrostatic fields and fly towards the respective detector (i.e., they follow one of the dashed lines).

II. METHODS

A. Experimental

The cooling dynamics of energized Np^+ and Az^+ were studied at the DESIREE infrastructure (FIG. 2). Separate samples of pure naphthalene or azulene (Sigma-Aldrich, >99%) were loaded into a resistively heated oven coupled ($T = 300\,K$) to an electron cyclotron resonance (ECR, Pantechnik Monogan) ion source with helium support gas. Note that the oven was not heated above ambient temperature, so there should be no thermal isomerization before ionization. Cations extracted from the source were accelerated to 34 keV kinetic energy, mass selected (m/z=128) using a 100° bending magnet (m/z resolution is sufficient to avoid selecting any m/z=127 dehydrogenated species produced in the ion source), and injected into the storage ring (orbit period $\approx 38\,\mu$s). The total ion transit time from the point of nascent ion formation in the source to injection into the storage ring was $\approx 100\,\mu$s, and $\approx 5\times10^4$ ions were injected each cycle (beam storage lifetime $\approx$500 s, which is typical for DESIREE experiments,[39,50–53] although the present experiments were performed out to $\approx$200 ms). After ion injection into the storage ring, neutral fragments formed in the lower straight section of the ring illustrated in FIG. 2 impact on the position sensitive 'Imaging Detector'.[54] This detector consists of ultra-high dynamic range micro-channel plates (MCPs, Photonis), suitable for high count rates at cryogenic temperatures, coupled with a phosphor screen. Ion neutralization images were recorded through a vac-

uum window using a CMOS camera (Photon Focus MV1-D2048) with 1.1 ms exposures every 2.5 ms. The images are time-stamped and synchronized with the storage cycle. In separate single-pass experiments, neutralization images providing KER distributions were recorded using a 0.5 mm aperture inserted before the straight section of the storage ring to reduce the smearing of the neutral distributions due to the spatial extent of the beam. Finally, we note that any dehydrogenated products formed in the storage ring (i.e., $[Az\text{-}H]^+$ and $[Np\text{-}H]^+$) are unlikely to undergo further C_2H_2 loss and, thus, contribute to the neutralization signal because such highly excited parent ions would not survive long enough to be injected into the ring.

Photo-induced experiments were performed by overlapping the stored ion beam with light ($11\,\mu J\,pulse^{-1}$, 250 Hz, unfocussed) from an EKSPLA NT-242 optical parametric oscillator (OPO) laser in a co-linear geometry in the upper straight section of the ring. The irradiation wavelengths at 415 nm (Np^+) and 425 nm (Az^+) were selected based on high absorption cross-sections in cold electronic spectra[55,56] and because of high laser fluence in this wavelength range.

B. Theoretical

1. Potential energy surfaces

Calculation of the isomerization and dissociation (mainly C_2H_2 elimination) potential energy surfaces (PESs) for Np^+ and Az^+ involved optimizing the minimum energy structures and transition states at the ωB97X-D/cc-pVTZ level of theory, followed by single-point energy calculations at the CCSD(T)/cc-pVTZ level of theory using Gaussian 16.B01.[57–60] Initial structures were taken from Ref. 35.

2. Isomerization and dissociation

Isomerization between Np^+ and Az^+, and dissociation by C_2H_2-elimination (and H-elimination for Np^+) were modeled using an RRKM (Rice–Ramsperger–Kassel–Marcus) equation

$$k(E) = \frac{\int_0^E \rho_t(E')dE'}{h\rho_r(E)} \tag{1}$$

where E is the vibrational energy, ρ_r and ρ_t are level densities for the reactant and transition state, respectively, and h is Planck's constant. On our relative energy scale, $E = 0$ corresponds to the ground state vibrational energy of Np^+. For all other structures, the level density starts (is non-zero) at the structure's ground state energy. Thus, the activation energies for each step are the differences between starting energies of ρ_r and ρ_t (as indicated by the prime).

3. Recurrent fluorescence

Recurrent fluorescence (RF), which is otherwise known as Poincaré fluorescence, corresponds to fluorescence emission from thermally populated electronic states.[41] The rate coefficient for RF, k_{RF}, was modeled using the expression:

$$k_{RF}(E) = A^{RF}\frac{\rho(E - h\nu_{el})}{\rho(E)} \tag{2}$$

where ρ is a density of states and ν_{el} is the electronic transition energy. The electronic Einstein coefficients, A^{RF}, were calculated by

$$A^{RF} = \frac{2\pi\nu_{el}^2 e^2}{\epsilon_0 m_e c^3} f \tag{3}$$

where f is the oscillator strength taken from Franck-Condon-Herzberg-Teller simulations at the LC-ωHPBE/cc-pVTZ level of theory within the TD-DFT framework.[61,62] Briefly, the low-lying electronic transitions of Np^+ have been determined using photoelectron and matrix-isolation spectroscopies,[55,63] with the first excited state ($^2B_{1u}$) at 0.73 eV and the second excited state ($^2B_{2g}$) situated between 1.93 and 1.84 eV. The first excited state is symmetry forbidden in absorption spectroscopy. Adjusting the experimental absorption value for vertical fluorescence transition energy based on our DFT calculations gave 1.66 eV. This value is in good agreement with the RF spectrum for Np^+ in Ref. 42. Spectroscopic investigations on Az^+ are more limited, although a photoelectron spectroscopy study of thermally-evaporated azulene has reported the first two electronic transitions at 1.09 and 2.66 eV.[64] For our RF simulations, we used the estimated fluorescence vertical transition energies combined with our calculated oscillator strengths at $f = 9.4\times10^{-2}$ for $D_2 \leftarrow D_0$ in Np^+ and $f = 1.7\times10^{-3}$, and 1.2×10^{-2} for $D_1 \leftarrow D_0$ and $D_2 \leftarrow D_0$ in Az^+, respectively.

4. IR emission

The infrared emission (vibrational cooling) rate coefficient, k_{IR}, for Np^+ and Az^+, were modeled assuming the simple harmonic cascade (SHC) approximation:[39]

$$k_{IR}(E) = \sum_s k_s = \sum_s A_s^{IR} \sum_{v=1}^{v\leq E/h\nu_s} \frac{\rho(E - vh\nu_s)}{\rho(E)} \tag{4}$$

where v is the vibrational quantum number, $h\nu_s$ is the transition energy, and A_s^{IR} is the Einstein coefficient for vibrational mode s taken from our calculations. The performance of this model has been discussed elsewhere,[39,65] but generally reproduces experimental data within a factor of two.

C. Master equation propagation

The time-dependent vibrational energy distribution, $g(E,t)$, initially normalized such that $\int g(E,t=0)dE = 1$, was propagated according to the Master equation

$$\frac{d}{dt}g(E,t) = -(k_{d,tot}(E) + k_{iso}(E))g(E,t) + \overline{k}_{iso}(E)\overline{g}(E,t) \sum_s [k_s(E+h\nu_s)g(E+h\nu_s,t) - k_s(E)g(E,t)] + k_{RF}(E+h\nu_{el})g(E+h\nu_{el},t) - k_{RF}(E)g(E,t). \quad (5)$$

In this expression, the first terms in parentheses describe depletion of the ion population by unimolecular dissociation (i.e., C_2H_2- and H-elimination) and isomerization, where the total dissociation rate coefficient is the sum of the rate coefficients for the various product channels (P), $k_{d,tot} = \sum_P k_{d,P}$. The next term is incoming population from the other isomer, with the overbars indicating the other isomer. The first term in brackets corresponds to $v+1 \rightarrow v$ vibrational emission from levels above E, while the second is associated with $v \rightarrow v-1$ emission to levels below E. The final two terms describe RF. The time step dt was chosen to match the experimental data, with 32 extra points prior to the first experimental time bin to allow for the ion transit time from the ion source to the storage ring. The simulated dissociation rate (assuming a constant beam population) for a given product channel is given by

$$\Gamma_P(t) = \int k_{d,P}(E)g(E,t)dE. \quad (6)$$

III. RESULTS AND DISCUSSION

A. Spontaneous cooling dynamics

Measured neutralization rates, $R(t)$, for Np^+ and Az^+ generated in the ECR source are shown in FIG. 3a. These data are averaged over more than 200,000 injection and storage cycles, and have a similar shape to those reported for other PAH cations.[51,66] Intriguingly, the measured storage time dependence of the neutralization rates for the two precursor ions appear near identical. In terms of the underlying physics of the neutralization rate curves, during the first $\approx 10^{-3}$ s after ion injection into the storage ring, the neutralization rate follows a power law trend, $R(t) \propto t^{-1}$, due to the broad distribution of internal energies, $[g(E,t)]$, of the ions and the rapid variation of the dissociation rate coefficient, $k_d(E)$, with E.[67] After a critical time (k_c^{-1}), dissociation is quenched by competition with radiative cooling (RF and IR),[68] resulting in a neutralization rate with approximate time dependence

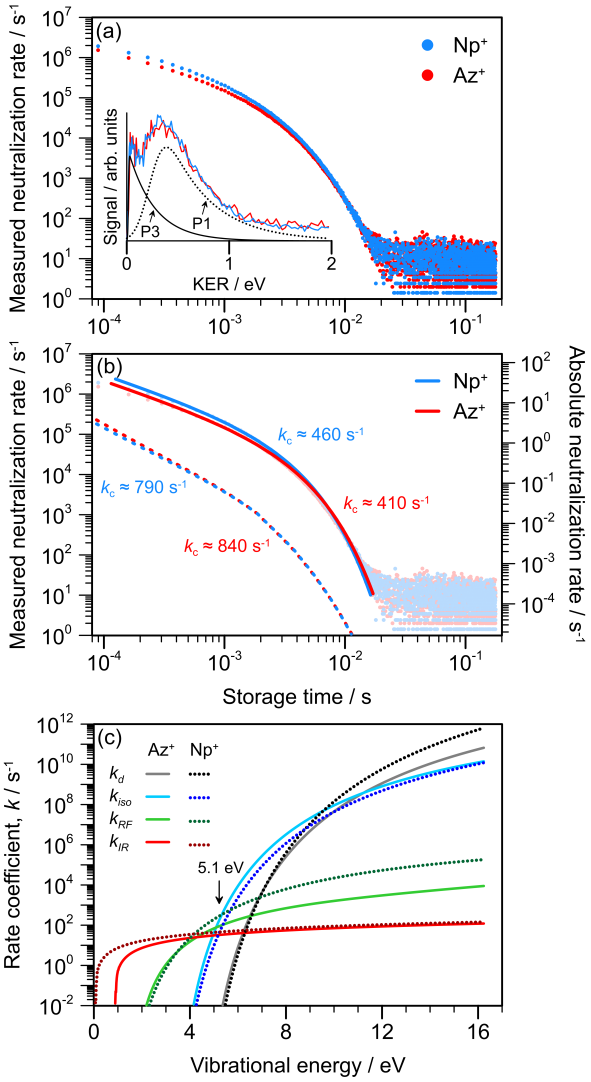

FIG. 3. Spontaneous neutralization of energized Np^+ and Az^+ produced in an ECR source: (a) measured neutralization rate with ion storage time, with single-pass kinetic energy release (KER) distributions shown in the inset, (b) fit of neutralization rate to EQN 6 (solid lines) and simulated absolute neutralization rate for Np^+ and Az^+ precursors (dashed lines), (c) simulated rate coefficients for C_2H_2-elimination (k_d), isomerization (k_{iso}), recurrent fluorescence (k_{RF}), and infrared cooling (k_{IR}). The average vibrational energy of the nascent ion ensembles is estimated at ≈5.1 eV, as indicated in (c). For (a) and (b), the measured neutralization rate is instrument dependent; absolute rates according EQN 9 are indicated on the right-hand vertical abscissa. In (c), the computed k_{RF} data are consistent with values in Ref. 42. Note the logarithmic scales on the vertical absicca of all panels, the and horizontal abscissas of (a) and (b).

$$R(t) = r_0 t^{-1} e^{-k_c t} \quad (7)$$

where r_0 is signal amplitude. The solid curves in FIG. 3b are fits of EQN 7 to the $R(t)$ data for $t >$

5×10^{-4} s. Extracted values of k_c are 460±30 s^{-1} (Np^+) and 410±30 s^{-1} (Az^+) and are comparable with those for 1-CNN^+ ($k_c = 300 \pm 20\,s^{-1}$)[15,44] and other larger PAH cations for which RF cooling is known to be important.[51,66,69] In contrast, k_c values for systems involving IR cooling alone are ≈100 s^{-1}. It should be also remembered that Np^+ is the PAH system for which RF has been conclusively observed.[42] Significantly, the k_c values for precursor Np^+ and Az^+ (as well as the cooling profiles) are similar, indicating similar dissociation and cooling dynamics (i.e., a common mechanism) over the fitted timescale. Application of the alternative fitting model

$$R(t) = r_0 t^{-\alpha} e^{-k_c t} \tag{8}$$

returned values of ≈500 s^{-1} for both ions, with values of α slightly less than unity. Deviation of α from unity (EQN 7) is attributed to a finite width internal energy distribution,[38,70] with $\alpha \approx 0$ corresponding to exponential-like decay of ions with a narrow and well-defined internal energy distribution. We return to discussing α values for the photo-induced neutralization data.

The $R(t)$ data presented in FIG. 3 are relative data that depend on instrumental factors. They are converted to absolute rates, $\Gamma(t)$, using the following expression determined from dimensional analysis of the DESIREE experiment

$$\Gamma(t) = \frac{f^2 q_e}{N_{cyc}\eta_{det} G I_{avg}} R(t) \tag{9}$$

where f = 23.87 kHz is the revolution frequency of the stored ions, q_e is the electron charge, I_{avg} = 300 pA (124 pA for Az^+) is the measured beam current at the end of the storage cycle, N_{cyc} = 213,177 (226,712 for Az^+) is the number of cycles, η_{det} = 0.4 is the detector efficiency,[15] and G = 0.11 is the fraction of the storage ring witnessed by the detector (note that the divergence of the neutral beam is dominated by KER).

KER distributions recorded by imaging neutral products formed during the first 100 μs after ions were injected into the ring are shown in the inset in FIG. 3a. The KER distributions associated with decomposition of Np^+ and Az^+ are essentially identical, providing some evidence that dissociation (and interlinked cooling dynamics) proceed through common mechanisms. Furthermore, there is little change in shape of the KER distribution over the first 10 ms of ion storage, indicating that a quasi-statistical $Np^+ \rightleftharpoons Az^+$ equilibrium is promptly established after ion generation in the ECR source. We use the term 'quasi-statistical' because not all ions possess internal energy in excess of isomerization and dissociation thresholds (FIG. 4). The KER distributions in FIG. 3a, inset, have a double-peaked structure with maxima at ≈0.05 eV and ≈0.4 eV, which differs from the Boltzmann-like KER distribution (peak maximum at ≈0.05 eV) recently measured for 1-CNN^+ using the same methodology.[15] Thus, there are multiple neutral formation (dissociation) pathways for the Np^+–Az^+ couple, which are not active for 1-CNN^+. As discussed below, these KER distributions are consistent with isomerization in concert with dissociation.

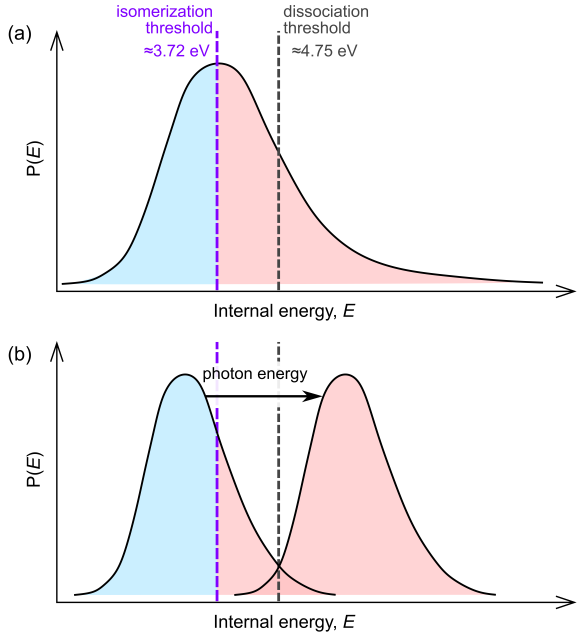

FIG. 4. Schematic illustrations of ion internal energy distributions, $[g(E,t)]$: (a) nascent Np^+ and Az^+ produced in the ECR source. Many of the ions are produced with high internal energies (red) in excess of the isomerization and dissociation threshold; these ions are subject to a competition between isomerization, dissociation, and cooling through RF and IR emission. A fraction of the nascent ions have internal energies lower than isomerization and dissociation thresholds (shaded blue), and may cool through IR and RF emission, without destruction through dissociation. The ions in the blue shaded region retain the precursor isomer structure and are those that become increasingly probed with ion storage time in the photo-induced experiments. (b) The blue population corresponds to stored ions that have cooled to some degree. This population contains both Np^+ and Az^+, but will be enriched in the precursor ion because of the blue fraction of the population in (a). Upon absorption of a visible photon (photo-induced experiments), the average internal energy is raised above the isomerization and dissociation thresholds.

B. Potential energy surfaces

To link the Np^+ and Az^+ cooling measurements with PESs for isomerization and dissociation, we recomputed the most probable PESs reported in the 2006 work by Dyakov *et al.*[35], who used RRKM theory to explore the importance of each pathway with internal energy. For isomerization, the norcaradiene-vinylidene (or

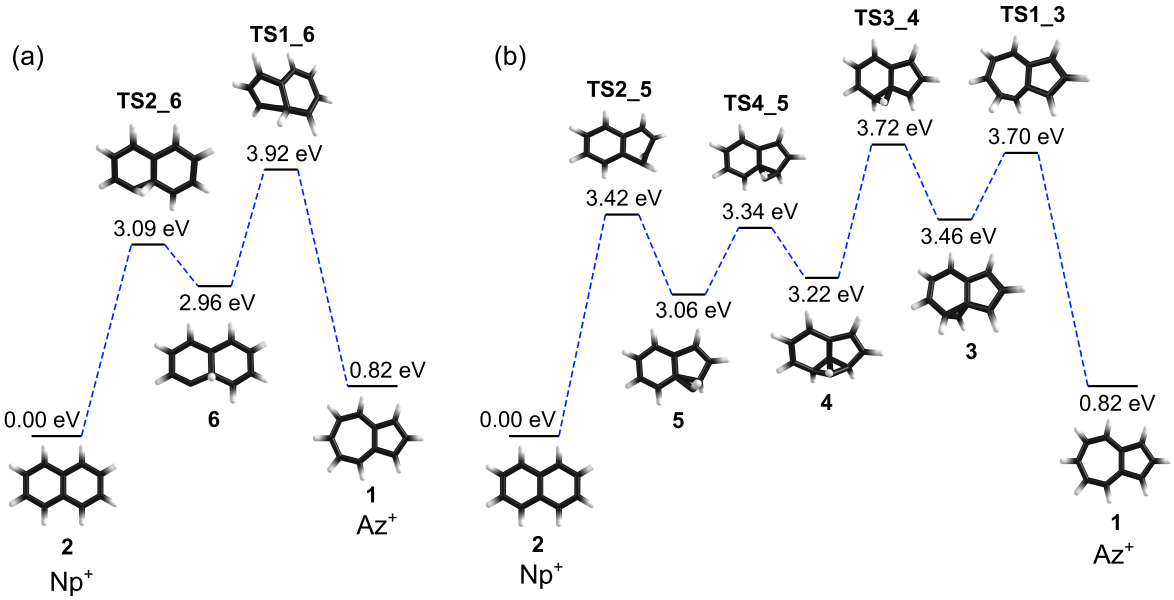

FIG. 5. Potential energy surfaces (CCSD(T)/cc-pVTZ) for Np^+ and Az^+ isomerization: (a) norcaradiene-vinylidene mechanism, (b) bicyclobutane mechanism. All energies are relative to Np^+. Labeling convention for the structures follows Ref. 35.

Dewar-Becker) mechanism[71,72] (FIG. 5a) is a two-step rearrangement, proceeding *via* a metastable, hydrogen-shifted naphthalene intermediate (species **6**). Conversely, the bicyclobutane isomerization mechanism[73] (FIG. 5b) is more complex, involving four transition states and three intermediates (species **3**, **4**, and **5**), although requires slightly lower activation energy. For dissociation leading to C_2H_2-elimination (FIG. 6a), the decomposition of Np^+ involves hydrogen shifts, followed by ring opening, forming the phenylacetylene cation (**P3**), which is the highest point (i.e., asymptotic) along the PES (4.75 eV, relative to Np^+). On the other hand, there are two feasible C_2H_2-elimination channels for Az^+ (FIG. 6b), sharing a slightly lower final barrier at 4.72 eV. In summary, our potential energy surfaces have the isomerization barriers at 3.92 eV (norcaradiene-vinylidene mechanism) and 3.72 eV (bicyclobutane mechanism), which are ≈1 eV lower than the C_2H_2-elimination barriers at 4.75 eV (**P3** product) and 4.72 eV (**P1** product). Our calculated values are within 0.1 eV of the earlier calculations by Dyakov *et al.*[35].

While experiments and supporting theoretical studies have demonstrated that C_2H_2- and H-elimination are the lowest energy dissociation pathways for the Np^+–Az^+ couple,[31,35,37] with approximately equal branching ratio at low excess internal energies (e.g., 1 eV above threshold), the imaging detector in DESIREE is not sensitive to H atoms,[66] so the KER distributions should reflect C_2H_2 formation. H-loss, if present, would be spread widely over the detector due to the low mass of H, and would be indistinguishable from background in the KER image. On the other hand, our master equation simulations combine all of these isomerization and dissociation PESs as well as an H-elimination channel (Supplementary Material). It is worth noting that a RRKM study on Np^+–Az^+ isomerization and dissociation dynamics calculated PESs using the B3LYP density functional (becoming obsolete) has been reported;[37] however, our coupled cluster PESs are in closer agreement with those in the Dyakov et al.[35] study, which employed the more robust G3(MP2,CC) method.

Returning to the KER distributions shown inset in FIG. 3a, we assigned the peak at ≈0.05 eV to Np^+-dissociation yielding **P3** since the C_2H_2-elimination pathway is asymptotic in relative energy. The KER peak centred at ≈0.4 eV is assigned to dissociation from Az^+ yielding **P1** where kinetic energy associated with dissociation is portioned between the two fragments and internal vibrational excitation due to intramolecular vibrational energy redistribution concerted with bond scission.

C. Master equation simulations

A key result from the spontaneous neutralization data is that 'low energy' dissociation (i.e., up to several eV above the dissociation threshold) from either Np^+ or Az^+ occurs through common pathways because the Np^+–Az^+ isomerization barriers are lower than those for C_2H_2-elimination.[24,28–32] To understand the interlink between isomerization, dissociation, and radiative cooling, we performed master equation simulations. The computed rates, using EQNS 1-4, the molecular structures and energies in FIG. 5 and 6, the vibrational frequencies (tabulated in the Supplementary Material), are shown in

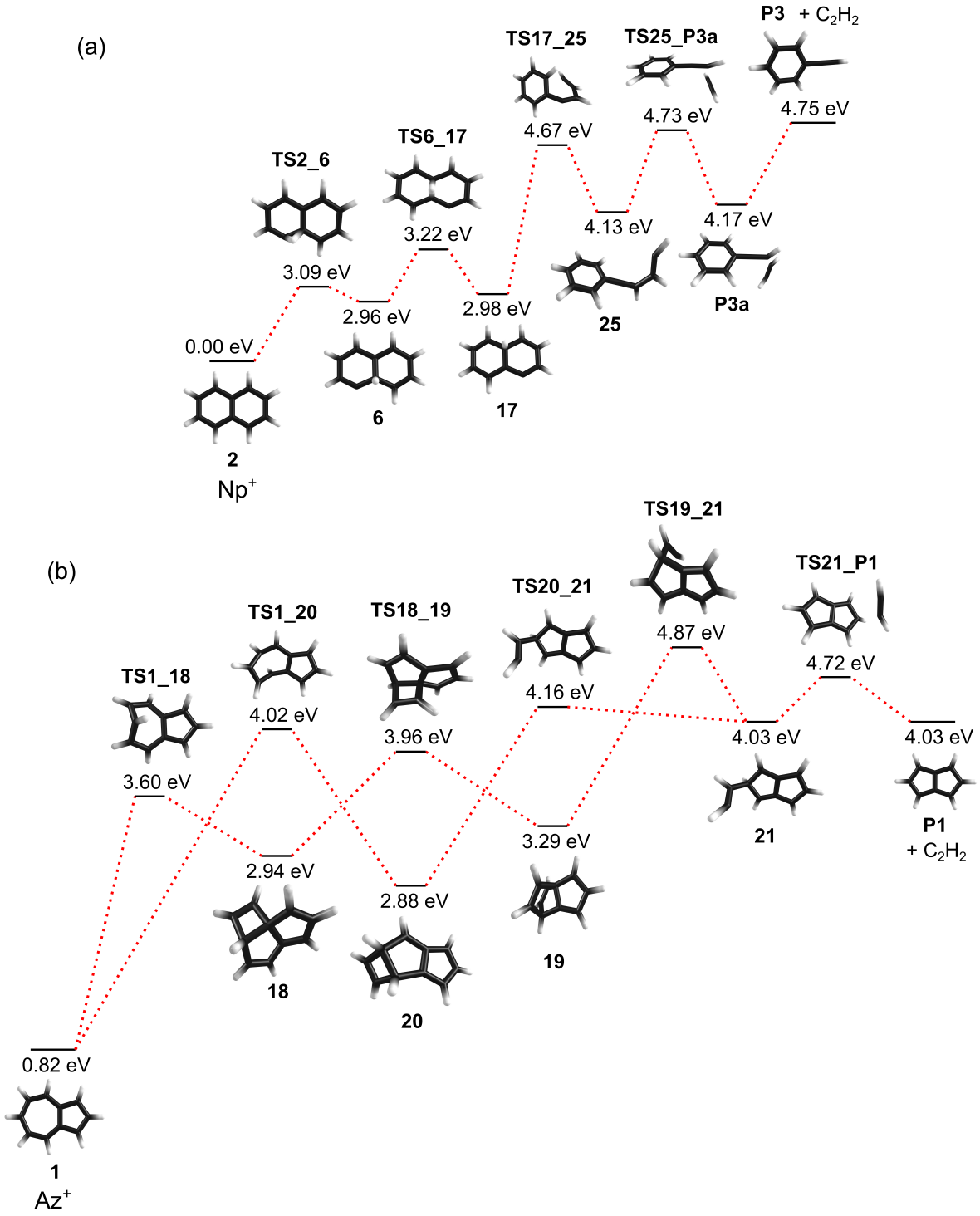

FIG. 6. Potential energy surfaces (CCSD(T)/cc-pVTZ) for dissociation (C_2H_2-elimination) from Np^+ and Az^+: (a) the phenylacetylene cation (**P3**) from Np^+, (b) the pentalene cation (**P1**) from Az^+. In (b), both pathways lead to P1, and both were included in the RRKM simulations. All energies are relative to Np^+. Labeling convention for the structures follows Ref. 35.

FIG. 3c. The total C_2H_2-elimination rate (EQN 6) from a simulation assuming initial vibrational energy distributions following Boltzmann statistics with the temperature $T = 1970\,\mathrm{K}$ for both isomers are shown in FIG. 3b. This temperature was chosen based on previous experiments with 1-CNN^+ using the same ion source and ion generation conditions.[15,44] The initial temperature of $T = 1970\,\mathrm{K}$ corresponds to an average vibrational energy of $\approx$5.1 eV, which is above the isomerization and dissociation barriers.

Returning to FIG. 3c, in accord with the Dyakov RRKM study,[35,36] there is an internal-energy-dependent branching between the two C_2H_2-elimination channels. The dissociation channel producing **P3** in FIG. 6a is important at low internal energies (<5.2 eV), while the channel producing **P1**, in FIG. 6b (red), becomes more important after the 'turnover region' at $\approx$5.2 eV. At internal energies greater than $\approx$9.5 eV, the branching ratio for the **P3** channel begins to increase slightly, while the ratio for the **P1** channel begins to decrease (this decrease being greater than the corresponding increase in species **P3**). At our initial simulated temperature that corresponds to $\approx$5.1 eV of vibrational energy, H-elimination and C_2H_2-elimination have roughly equal probability, with a 75%:25% branching between **P3** and **P1** products for C_2H_2-elimination. This C_2H_2-elimination channel branching is consistent with the 70%:30% ($\pm$10% uncertainty) ratio determined from a fit of the single-pass KER distributions (dashed lines in FIG. 3a, inset).

D. Radiative cooling

The simulations in FIG. 3c indicate that RF cooling has the largest rate constant in the 4–5 eV internal energy range, with Np^+ being more efficient at RF than Az^+. This energy range spans the UV absorption bands in both ions. For internal energies below $\approx$4 eV, cooling is dominated by IR emission. The computed cooling rates for RF and IR are comparable with those determined for 1-CNN^+,[15,44] although RF cooling is slightly less efficient for Np^+ compared with 1-CNN^+ for vibrational energies <6 eV. The reduced rate of RF for Np^+, even though the oscillator strength $f = 9.4 \times 10^{-2}$ is substantially larger than $f = 1.1 \times 10^{-2}$ for 1-CNN^+, is because of the higher RF transition energy for Np^+ at $\approx$1.6 eV compared with the calculated value of 1.10 eV for 1-CNN^+. We note that our simulated RF rates for Np^+ are similar to those reported by Saito et al. [42].

Fits of the simulated neutralization curves to EQN 7, shown in FIG. 3b, returned k_c values of $790\pm10\,\mathrm{s}^{-1}$ for Np^+ and $840\pm10\,\mathrm{s}^{-1}$ for Az^+, which are 1.7–2-fold larger than the fitted values for the experimental data. This indicates that the quenching of dissociation by radiative cooling is slightly overestimated by the model. Interestingly, the simulated absolute neutralization rates shown in FIG. 3b are about an order of magnitude lower than the (absolute) experimental data. We have applied similar master equation simulation methodology to describe the spontaneous cooling profiles for other PAH cations and found better agreement between absolute experimental rates, although these systems were not complicated by isomerization dynamics or multiple dissociation pathways.[15,44,51,66] Potential reasons for the difference in absolute rates in this work include: (i) the simulations assume a Boltzmann distribution with some average temperature; however, the true nascent ion temperature distribution may differ and have a different shape on the low temperature side, for example, see Ref. 42 for an alternative internal energy distribution (although the distribution will be ion source and instrument specific), and (ii) the PESs for dissociation are complicated – our simulations considered only the lowest energy pathways for isomerization and elimination of C_2H_2, while theory has predicted several other pathways that may be cumulative.[35,37] Still, we conclude that the simulations are able to reasonably reproduce the experimental trends.

E. Photo-induced cooling dynamics

In addition to monitoring spontaneous neutralization of energized Np^+ and Az^+, we performed photo-induced neutralization experiments. These experiments involved irradiating the stored ions with 415 nm (Np^+) or 425 nm (Az^+) light every 4 ms. One may think of the photo-induced experiment as depositing a known amount of energy, 3.0 eV for Np^+ and 2.9 eV for Az^+, into the cooling ensemble (since internal conversion dynamics are fast compared with all other dynamics occurring on the ground electronic state) – see FIG. 4b. The photo-induced cooling profile, averaged over many storage cycles, associated with the first 15 laser irradiations for Np^+ is shown in FIG. 7a. The inset shows the photo-induced responses for several cycles corrected for the spontaneous neutralization background (i.e., no laser). Integrated neutralization yields with time after laser firing were fit EQN 8 with k_c fixed at $460\,\mathrm{s}^{-1}$, as determined from the spontaneous decay measurements for Np^+ (and not sensitive to using $410\,\mathrm{s}^{-1}$). The assumption of a fixed k_c is warranted because these experiments were conducted with a low laser power resulting in only single-photon absorption. Furthermore, absorption of a single $\approx$3 eV photon provides insufficient internal energy to heat cold (e.g., near ground vibrational state) ions above the dissociation threshold. Consequently, the ions probed with the laser must have more than $\approx$2 eV of internal energy. The integrated neutralization yields with time after laser firing for five selected ions storage times used for the fits to extract α values are shown in FIG. 7c (Np^+) and FIG. 7d (Az^+) as log-log plots, and in FIG. 7e (Np^+) and FIG. 7f (Az^+) as semi-log plots. The purpose of the semi-log plots are to show that the decay of the neutral signal roughly follows a linear trend $\approx$0.8 ms after laser firing, consistent with α tending towards zero.

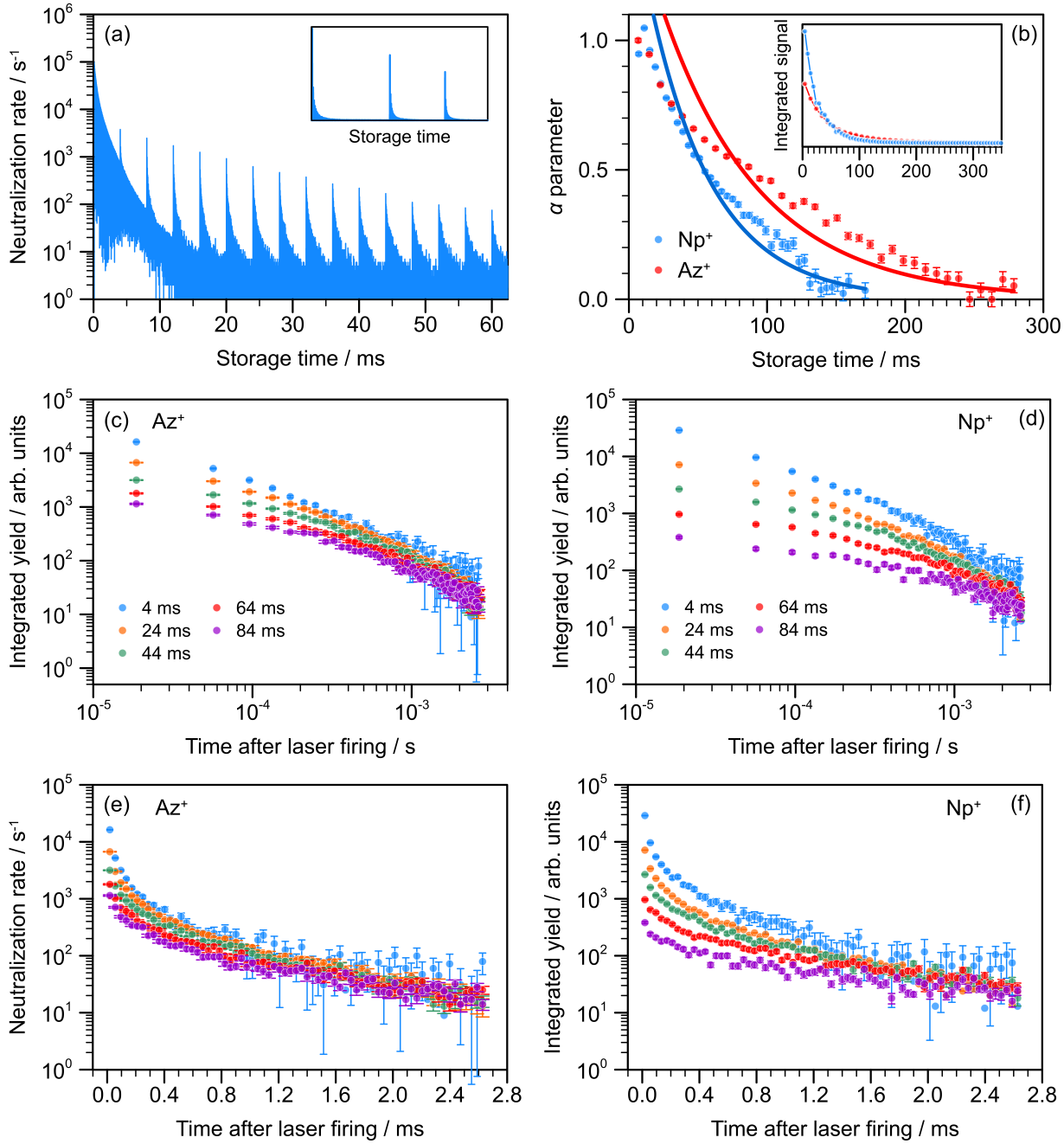

FIG. 7. Photo-induced neutralization of Np^+ and Az^+ with ion storage time: (a) Example neutralization rate curve for Np^+ showing the first 15 laser irradiations using 415 nm light. Background corrected in the inset. (b) Values of fitted parameter α for the Np^+ and Az^+ irradiated cooling profiles. Exponential decay fits are included as a guide. The inset shows the integrated laser-induced neutralization yield with ion storage time. (c) Background-corrected neutralization rates (log-log) for five selected laser irradiations of source-heated Np^+. (d) Background-corrected neutralization rates (log-log) for five selected laser irradiations of source-heated Az^+. (e) and (f) semi-log plots of the data in (c) and (d), respectively.

Values of α obtained from fits of EQN 8 are given in FIG. 7b, revealing an exponential-like decrease in magnitude with ion storage time, corresponding to cooling and narrowing of the vibrational energy distribution associated with the ions excited by the laser pulse. Significantly, while the precursor Np^+ and Az^+ species gave similar values of α for short ion storage times (e.g., 0–50 ms), they start to deviate for longer ion storage times, indicating distinct cooling dynamics. Our interpretation is that, as the ion ensemble cools, the vibrational energy distribution illustrated in FIG. 4a evolves into the situation illustrated in FIG. 4b. Specifically, as the ion ensem-

ble cools, many of the energized ions possessing an internal vibrational energy above the ionization and dissociation thresholds are lost through dissociation, leaving the cooler part of the ion ensemble enriched with the precursor isomer. The deviation of the trend in α, thus, reflects differences in radiative cooling (RF and IR) between the two precursor ions. Because α values for Np^+ have a steeper decrease with ion storage time than for Az^+, we conclude that RF cooling is more efficient for Np^+. This conclusion is consistent with both the fitted experimental k_c values in FIG. 3b (slightly larger for Np^+) and the simulations in FIG. 3c, where for $E > 3\,eV$, the computed k_{RF} value for Np^+ is larger than that for Az^+. This conclusion is further supported by the integrated laser-induced neutralization signal with ion stage time shown inset in FIG. 7b, where Np^+ exhibits a steeper decay than that for Az^+.

It is important to remember that, because the photon energy at ≈3 eV used in the above experiments is well below the dissociation barriers (≈4.7 eV), the laser-induced signal is associated with the fraction of ions possessing internal energies of more than ≈2 eV; excitation of cold ions would not provide sufficient internal energy for those ions to dissociate. The tendency of the fitted α values from ≈1 at short storage times to ≈0 at longer storage times, thus, corresponds to the fraction of ions in the high internal energy tail of the nascent ion thermal distribution, rather than the entire thermal distribution.

IV. ASTROCHEMICAL SIGNIFICANCE

For several decades, PAHs have been thought to be ubiquitous in the interstellar medium and to dominate the IR emission bands observed by astronomers at wavelengths coincident with PAH vibrational transition energies.[5,74–76] Interestingly, many IR bands show only small variations across astrochemical environments,[77] leading to the conclusion that these environments contain either a common subset of PAHs,[78] or a high diversity of PAHs that result in the same average spectrum.[79] These emission bands are ubiquitous in the universe, observed in many astrochemical environments (predominantly UV-irradiated), including the galactic interstellar medium, planetary nebulae, star forming regions, and other galaxies.[80,81] However, because they cannot be used to identify specific molecular species, it is desirable to have experimental characterizations of the cooling dynamics and IR emission properties of prototype PAHs. The conventional wisdom was that PAHs possessing less than ca. 50 atoms would not possess the ability to radiatively stabilize in space and would decompose.[12–14] However, the discovery of two isomers of cyanonaphthalene and the indene molecules in TMC-1, albeit a cold, dark environment, challenge this wisdom.[11,16,17] Intriguingly, the observed abundances of the cyanonaphthalenes are six orders of magnitude higher than could be explained by standard astrochemical modeling involving growth mechanisms assuming a 'bottom-up' model from naphthalene. One hypothesis put forward by McGuire *et al.*[11] to explain the high abundance of cyanonaphthalenes in TMC-1 is that a larger-than-expected amount of naphthalene was inherited from the diffuse interstellar medium at early stages of cloud formation. RF-enhanced stability of naphthalene is consistent with this hypothesis. As detailed in our recent study on 1-CNN^+,[15,44] part of the abundance discrepancy is likely because the destruction rate assumed in the model is too high; the model considered radiative stabilization effectuated by only IR emission, not through faster RF cooling, which is known to occur for Np^+.[42]

Despite isolated PAHs in space spending most of their lives as an internally cold molecule, a key requirement for a PAH to be carrier of IR bands is that they must survive any rare instances of collisional (thermal) heating such as from shock waves, and photo-induced heating (e.g., UV absorption or 13.6 eV H-ionization radiation in photodissociation regions). Photoresilience requires the molecule to liberate energy in a manner that suppresses dissociation (i.e., radiative cooling). As shown in this work, while some fraction of energized Np^+ and Az^+ dissociate, RF leads to an appreciable fraction becoming stabilized and dissociation being suppressed). Thus, in accord with recent studies on 1-CNN^+, we reaffirm that RF is important for radiative stabilization of small PAHs, and that 'bottom-up' PAH growth models, like that assumed for cyanonaphthalene growth,[11] are likely astrochemical pathways. To help place the importance of radiative cooling into context, we plot ion survival probability with internal energy in FIG. 8. While dissociation thresholds are ≈4.8 eV, our simulations predict a near 100% survival rate of ions with internal vibrational energy <5.8 eV, with a small fraction of ions surviving with internal energies up to ≈7 eV. Because the ionization potential of neutral naphthaene is 8.144±0.001 eV[82] and Np^+ can withstand <5.8 eV of vibrational energy, neutral naphthalene molecules should retain their organic backbone following ionization by 13.6 eV H-ionization radiation. In contrast, the survival probability curve for 1-CNN^+ is shifted to ≈1 eV lower vibrational energy due to a lower dissociation threshold of ≈3 eV.[83] This interpretation for naphthalene is consistent with the iPEPICO results from West et al.[31], which show no appreciable fragmentation of naphthalene below 15 eV photon energies, although those experiments sampled shorter times after ionization than the present experiments and they may be subject to a kinetic shift.

Azulene has not been detected in space by the same radioastronomy surveys that identified the two CNN isomers, indene, and 2-cyanoindene.[11,16,17] While this may be due to the low dipole moment of azulene, it is consistent with the present results showing that Az^+ excited by 5–7 eV converts to Np^+, and is then stabilized by RF. This process, and the equivalent one in the neutrals, would enrich naphthalene compared with azulene.

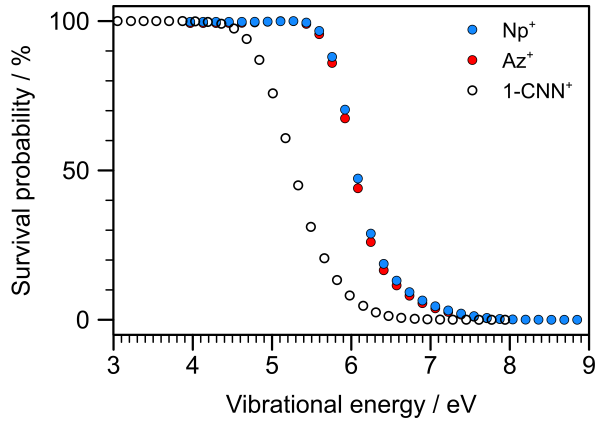

FIG. 8. Ion survival probability with internal energy from the master equation simulations. Data for 1-CNN^+ are taken from Ref. 15. The higher survival probability for Np^+–Az^+ compared with 1-CNN^+ over the 5–8 eV range is attributed to higher dissociation thresholds in the former.

V. CONCLUSIONS

The measurements and theory reported in this work are consistent with the establishment of an isomerization equilibrium between Np^+ and Az^+ generated in a thermal source, which precedes dissociation. Our ion storage ring measurements, which are supported by statistical modeling, provide characterization of the radiative cooling and associated dynamics over timescales relevant to $C_{10}H_8$ ions present in certain astrochemical environments. Access to these ultraslow timescales is afforded by conducting experiments under 'molecular cloud in a box' conditions. Master equation simulations are able to reproduce the radiative cooling properties of the ions and demonstrate that RF is the dominant non-destructive cooling mechanism. In accord with a recent study on 1-cyanonaphthalene radical cations by some of the present authors,[15,44] we reaffirm that RF cooling is an important radiative cooling mechanism for the photoresilience of small PAHs in space. These findings help to account for the anomalous observed abundances of small PAHs in TMC-1, where their preponderance exceeds predictions from astrochemical models.

Although Np^+ and Az^+ are the 'simplest' PAH cations, in many regards, they present the most complex PAH system studied at DESIREE so far, due to clear signatures for a competition between isomerization, dissociation, and radiative cooling. This complexity is because isomerization barriers are lower than dissociation barriers. Similar situations may exist for a range of other PAH systems,[84–86] including ring-expanded *vs* ring-methylated PAHs, and PAHs containing an azulene-like moiety with an extended and a contracted ring.[83] Specific examples include radical cations of the anthracene-phenanthrene couple and the related $C_{13}H_9N^+$ system,[87–89] and isomers of pyrene and coronene.[90,91] Also of note is that similar isomerization dynamics, particularly involving hydrogen-shifts, might be common for PAHs with varying degrees of dehydrogenation.[84]

The methodology applied in this work, involving generating and storing hot radical cations, and probing their spontaneous thermal and photo-induced cooling dynamics, can readily be extended to many of the systems noted above. However, future experiments, ideally, would focus on photo-induced cooling dynamics, for either open or closed shell ions, as a function of excitation wavelength, starting with internally-cold ions. The appeal of photo-induced experiments stems from the ability to deliver a precise amount of energy, provided that excitation is followed by prompt internal conversion to recover the ground electronic state (usually picoseconds in isolated PAHs)[24–27] and that ensuing intramolecular energy redistribution is rapid. Such experiments might best be conducted using a new electrospray ionization source available at DESIREE that incorporates a cryogenic pre-trap to cool ions before they are injection into the storage ring. This pre-cooling provides an internal energy distribution more similar to FIG. 4b, thereby avoiding waiting for hot ions produced in thermal sources to cool. For Np^+ and Az^+, provided they could be satisfactorily generated through electrospray ionization, this approach should provide near-pure ensembles of each isomer, avoiding the complications associated with coexisting isomers at the start of each ion storage cycle. For pure isomer ensembles, measurement of KER distributions as a function of excitation energy would provide a rigorous probe of PES barriers to isomerization and calibration of the master equation simulation methodology currently used to model cooling dynamics.

SUPPLEMENTARY MATERIAL

The Supplementary Material contains details on: H and H_2 elimination channels, calculated vibrational frequencies, and optimized molecular geometries.

DATA AVAILABILITY

The data that support the findings of this study are available from the corresponding author and DESIREE facility upon reasonable request.

ACKNOWLEDGMENTS

Funding was provided by the Swedish Foundation for International Cooperation in Research and Higher Education (STINT) Grant for Internationalisation programme (PT2017-7328 to MHS and JNB), and an EPSRC New Investigator Award (EP/W018691 to JNB). JWLL acknowledges financial support from the

Helmholtz-ERC Recognition Award (ERC-RA-0043) of the Helmholtz Association (HGF). EKA thanks the University of East Anglia for doctoral studentship. Electronic structure calculations were carried out on the High Performance Computing Cluster supported by the Research and Specialist Computing Support service at the University of East Anglia. HZ and HTS thank the Swedish Research Council for individual project grants (with contract Nos. 2020-03437 and 2022-02822). We acknowledge the DESIREE infrastructure for provisioning of facilities and experimental support, and thank the operators and technical staff. The DESIREE infrastructure receives funding from the Swedish Research Council under the Grant numbers 2017-00621 and 2021-00155. This article is based upon work from COST Action CA18212 – Molecular Dynamics in the GAS phase (MD-GAS), supported by COST (European Cooperation in Science and Technology). Nikolaj Klinkby is thanked for useful discussions and assistance in statistical data analysis.

AUTHOR CONTRIBUTIONS

This work was based on a beamtime application prepared by JWLL, MHS, and JNB. JWL, MHS, JENN, EG, DG, MCJ, BZ, SI, and JNB participated in experimental data acquisition. HZ and HTS managed the DESIREE facility. Analysis of experimental data was performed by JENN, MHS, EKA, and JNB. RRKM and master equation simulations were performed by MHS. Electronic structure calculations were performed by EKA and JNB. The manuscript was prepared by JNB with assistance from MHS and EKA, and was discussed by all authors.

CONFLICTS OF INTEREST

The authors have no conflicts to disclose.

REFERENCES

[1]G. Liu, Z. Niu, D. V. Niekerk, J. Xue, and L. Zheng, in *Reviews of Environmental Contamination and Toxicology* (Springer New York, 2008) pp. 1–28.
[2]M. Howsam and K. C. Jones, in *The Handbook of Environmental Chemistry* (Springer Berlin Heidelberg, 1998) pp. 137–174.
[3]T. Henning and F. Salama, Science **282**, 2204 (1998).
[4]A. G. G. M. Tielens, Rev. Mod. Phys. **85**, 1021 (2013).
[5]A. G. G. M. Tielens, Ann. Rev. Astron. Astrophys. **46**, 289 (2008).
[6]E. Peeters, Proc. Int. Astron. Union **7**, 149 (2011).
[7]S. Kwok and Y. Zhang, Nature **479**, 80 (2011).
[8]G. Lagache, H. Dole, J.-L. Puget, P. G. Perez-Gonzalez, E. L. Floc'h, G. H. Rieke, C. Papovich, E. Egami, A. Alonso-Herrero, C. W. Engelbracht, K. D. Gordon, K. A. Misselt, and J. E. Morrison, Astrophys. J. Supp. Ser. **154**, 112 (2004).
[9]J. D. T. Smith, B. T. Draine, D. A. Dale, J. Moustakas, J. R. C. Kennicutt, G. Helou, L. Armus, H. Roussel, K. Sheth, G. J. Bendo, B. A. Buckalew, D. Calzetti, C. W. Engelbracht, K. D. Gordon, D. J. Hollenbach, A. Li, S. Malhotra, E. J. Murphy, and F. Walter, Astrophys. J. **656**, 770 (2007).
[10]A. Li, Nat. Astron. **4**, 339 (2020).
[11]B. A. McGuire, R. A. Loomis, A. M. Burkhardt, K. L. K. Lee, C. N. Shingledecker, S. B. Charnley, I. R. Cooke, M. A. Cordiner, E. Herbst, S. Kalenskii, M. A. Siebert, E. R. Willis, C. Xue, A. J. Remijan, and M. C. McCarthy, Science **371**, 1265 (2021).
[12]M. Rapacioli, F. Calvo, C. Joblin, P. Parneix, D. Toublanc, and F. Spiegelman, Astron. Astrophys. **460**, 519 (2006).
[13]J. Montillaud, C. Joblin, and D. Toublanc, Astron. Astrophys. **552**, A15 (2013).
[14]M. Chabot, K. Béroff, E. Dartois, T. Pino, and M. Godard, Astrophys. J. **888**, 17 (2019).
[15]M. H. Stockett, J. N. Bull, H. Cederquist, S. Indrajith, M. Ji, J. E. Navarro Navarrete, H. T. Schmidt, H. Zettergren, and B. Zhu, Nat. Comm. **14**, 395 (2023).
[16]A. M. Burkhardt, K. L. K. Lee, P. B. Changala, C. N. Shingledecker, I. R. Cooke, R. A. Loomis, H. Wei, S. B. Charnley, E. Herbst, M. C. McCarthy, and B. A. McGuire, Astrophys. J. Lett. **913**, L18 (2021).
[17]M. L. Sita, P. B. Changala, C. Xue, A. M. Burkhardt, C. N. Shingledecker, K. L. K. Lee, R. A. Loomis, E. Momjian, M. A. Siebert, D. Gupta, E. Herbst, A. J. Remijan, M. C. McCarthy, I. R. Cooke, and B. A. McGuire, Astrophys. J. Lett. **938**, L12 (2022).
[18]L. Verstraete, EAS Publications Series **46**, 415 (2011).
[19]E. L. O. Bakes and A. G. G. M. Tielens, Astrophys. J. **427**, 822 (1994).
[20]J. C. Weingartner and B. T. Draine, Astrophys. J. Supp. Ser. **134**, 263 (2001).
[21]I. Kamp and C. P. Dullemond, Astrophys. J. **615**, 991 (2004).
[22]E. Heilbronner, P. A. Plattner, and K. Wieland, Experientia **3**, 70 (1947).
[23]M. S. Mirzaei, A. A. Taherpour, and C. Wentrup, J. Org. Chem. **87**, 3296 (2022).
[24]W. Cui, B. Hadas, B. Cao, and C. Lifshitz, J. Phys. Chem. A **104**, 6339 (2000).
[25]L. Zhao, R. Lian, I. A. Shkrob, R. A. Crowell, S. Pommeret, E. L. Chronister, A. D. Liu, and A. D. Trifunac, J. Phys. Chem. A **108**, 25 (2003).
[26]G. Reitsma, J. Hummert, J. Dura, V. Loriot, M. J. J. Vrakking, F. Lépine, and O. Kornilov, J. Phys. Chem. A **123**, 3068 (2019).
[27]J. W. L. Lee, D. S. Tikhonov, P. Chopra, S. Maclot, A. L. Steber, S. Gruet, F. Allum, R. Boll, X. Cheng, S. Düsterer, B. Erk, D. Garg, L. He, D. Heathcote, M. Johny, M. M. Kazemi, H. Köckert, J. Lahl, A. K. Lemmens, D. Loru, R. Mason, E. Müller, T. Mullins, P. Olshin, C. Passow, J. Peschel, D. Ramm, D. Rompotis, N. Schirmel, S. Trippel, J. Wiese, F. Ziaee, S. Bari, M. Burt, J. Küpper, A. M. Rijs, D. Rolles, S. Techert, P. Eng-Johnsson, M. Brouard, C. Vallance, B. Manschwetus, and M. Schnell, Nat. Comm. **12**, 6107 (2021).
[28]R. Stolze and H. Budzikiewicz, Monatsh. Chem. **109**, 325 (1978).
[29]H. Jochims, H. Rasekh, E. Rühl, H. Baumgärtel, and S. Leach, Chem. Phys. **168**, 159 (1992).
[30]K. Schroeter, D. Schröder, and H. Schwarz, J. Phys. Chem. A **103**, 4174 (1999).
[31]B. West, C. Joblin, V. Blanchet, A. Bodi, B. Sztáray, and P. M. Mayer, J. Phys. Chem. A **116**, 10999 (2012).
[32]J. Bouwman, A. J. de Haas, and J. Oomens, Chem. Comm. **52**, 2636 (2016).
[33]U. Jacovella, C. Rossi, C. Romanzin, C. Alcaraz, and R. Thissen, ChemPhysChem **24**, e202200474 (2023).
[34]G. Koster, J. M. L. Martin, and C. Lifshitz, J. Chem. Soc. Perkin Trans. 2 , 2383 (1999).
[35]Y. A. Dyakov, C.-K. Ni, S. H. Lin, Y. T. Lee, and A. M. Mebel, Phys. Chem. Chem. Phys. **8**, 1404 (2006).
[36]Y. A. Dyakov, A. M. Mebel, S. H. Lin, Y. T. Lee, and C.-K. Ni, J. Chinese Chem. Soc. **53**, 161 (2006).
[37]E. A. Solano and P. M. Mayer, J. Chem. Phys. **143**, 104305 (2015).

[38] J. Bernard, L. Chen, R. Brédy, M. Ji, C. Ortéga, J. Matsumoto, and S. Martin, Nucl. Instrum. Meth. Phys. Res. B **408**, 21 (2017).
[39] J. N. Bull, M. S. Scholz, E. Carrascosa, M. K. Kristiansson, G. Eklund, N. Punnakayathil, N. de Ruette, H. Zettergren, H. T. Schmidt, H. Cederquist, and M. H. Stockett, J. Chem. Phys. **151**, 114304 (2019).
[40] A. Nitzan and J. Jortner, J. Chem. Phys. **71**, 3524 (1979).
[41] A. Léger, P. Boissel, and L. d'Hendecourt, Phys. Rev. Lett. **60**, 921 (1988).
[42] M. Saito, H. Kubota, K. Yamasa, K. Suzuki, T. Majima, and H. Tsuchida, Phys. Rev. A **102**, 012820 (2020).
[43] R. D. Thomas, H. T. Schmidt, G. Andler, M. Björkhage, M. Blom, L. Brännholm, E. Bäckström, H. Danared, S. Das, N. Haag, P. Halldén, F. Hellberg, A. I. S. Holm, H. A. B. Johansson, A. Källberg, G. Källersjö, M. Larsson, S. Leontein, L. Liljeby, P. Löfgren, B. Malm, S. Mannervik, M. Masuda, D. Misra, A. Orbán, A. Paál, P. Reinhed, K.-G. Rensfelt, S. Rosén, K. Schmidt, F. Seitz, A. Simonsson, J. Weimer, H. Zettergren, and H. Cederquist, Rev. Sci. Instrum. **82**, 065112 (2011).
[44] J. E. Navarro Navarrete, J. N. Bull, H. Cederquist, S. Indrajith, M. Ji, H. T. Schmidt, H. Zettergren, B. Zhu, and M. H. Stockett, Faraday Discuss. 10.1039/D3FD00005B (2023).
[45] M. J. Jensen, U. V. Pedersen, and L. H. Andersen, Phys. Rev. Lett. **84**, 1128 (2000).
[46] K. Saha, V. Chandrasekaran, O. Heber, M. A. Iron, M. L. Rappaport, and D. Zajfman, Nat. Comm. **9**, 912 (2018).
[47] A. K. Lemmens, D. B. Rap, J. M. M. Thunnissen, B. Willemsen, and A. M. Rijs, Nat. Comm. **11**, 269 (2020).
[48] H. T. Schmidt, H. A. Johansson, R. D. Thomas, W. D. Geppert, N. Haag, P. Reinhed, S. Rosén, M. Larsson, H. Danared, K.-G. Rensfelt, L. Liljeby, L. Bagge, M. Björkhage, M. Blom, P. Löfgren, A. Källberg, A. Simonsson, A. Paál, H. Zettergren, and H. Cederquist, Int. J. Astrobio. **7**, 205 (2008).
[49] H. Kreckel, O. Novotný, and A. Wolf, Phil. Trans. Roy. Soc. A **377**, 20180412 (2019).
[50] H. T. Schmidt, R. D. Thomas, M. Gatchell, S. Rosén, P. Reinhed, P. Löfgren, L. Brännholm, M. Blom, M. Björkhage, E. Bäckström, J. D. Alexander, S. Leontein, D. Hanstorp, H. Zettergren, L. Liljeby, A. Källberg, A. Simonsson, F. Hellberg, S. Mannervik, M. Larsson, W. D. Geppert, K. G. Rensfelt, H. Danared, A. Paál, M. Masuda, P. Halldén, G. Andler, M. H. Stockett, T. Chen, G. Källersjö, J. Weimer, K. Hansen, H. Hartman, and H. Cederquist, Rev. Sci. Instrum. **84**, 055115 (2013).
[51] M. H. Stockett, J. N. Bull, J. T. Buntine, E. Carrascosa, M. Ji, N. Kono, H. T. Schmidt, and H. Zettergren, J. Chem. Phys. **153**, 154303 (2020).
[52] M. H. Stockett, J. N. Bull, H. T. Schmidt, and H. Zettergren, Phys. Chem. Chem. Phys. **24**, 12002 (2022).
[53] E. Bäckström, D. Hanstorp, O. M. Hole, M. Kaminska, R. F. Nascimento, M. Blom, M. Björkhage, A. Källberg, P. Löfgren, P. Reinhed, S. Rosén, A. Simonsson, R. D. Thomas, S. Mannervik, H. T. Schmidt, and H. Cederquist, Phys. Rev. Lett. **114**, 143003 (2015).
[54] S. Rosén, H. T. Schmidt, P. Reinhed, D. Fischer, R. D. Thomas, H. Cederquist, L. Liljeby, L. Bagge, S. Leontein, and M. Blom, Rev. Sci. Instrum. **78**, 113301 (2007).
[55] F. Salama and L. J. Allamandola, J. Chem. Phys. **94**, 6964 (1991).
[56] T. Pino, N. Boudin, and P. Bréchignac, J. Chem. Phys. **111**, 7337 (1999).
[57] J.-D. Chai and M. Head-Gordon, Phys. Chem. Chem. Phys. **10**, 6615 (2008).
[58] T. H. Dunning, J. Chem. Phys. **90**, 1007 (1989).
[59] J. A. Pople, M. Head-Gordon, and K. Raghavachari, J. Chem. Phys. **87**, 5968 (1987).
[60] M. J. Frisch, G. W. Trucks, H. B. Schlegel, G. E. Scuseria, M. A. Robb, J. R. Cheeseman, G. Scalmani, V. Barone, B. Mennucci, G. A. Petersson, H. Nakatsuji, M. Caricato, X. Li, H. P. Hratchian, A. F. Izmaylov, J. Bloino, G. Zheng, J. L. Sonnenberg, M. Hada, M. Ehara, K. Toyota, R. Fukuda, J. Hasegawa, M. Ishida, T. Nakajima, Y. Honda, O. Kitao, H. Nakai, T. Vreven, J. A. Montgomery, Jr., J. E. Peralta, F. Ogliaro, M. Bearpark, J. J. Heyd, E. Brothers, K. N. Kudin, V. N. Staroverov, R. Kobayashi, J. Normand, K. Raghavachari, A. Rendell, J. C. Burant, S. S. Iyengar, J. Tomasi, M. Cossi, N. Rega, J. M. Millam, M. Klene, J. E. Knox, J. B. Cross, V. Bakken, C. Adamo, J. Jaramillo, R. Gomperts, R. E. Stratmann, O. Yazyev, A. J. Austin, R. Cammi, C. Pomelli, J. W. Ochterski, R. L. Martin, K. Morokuma, V. G. Zakrzewski, G. A. Voth, P. Salvador, J. J. Dannenberg, S. Dapprich, A. D. Daniels, Ö. Farkas, J. B. Foresman, J. V. Ortiz, J. Cioslowski, and D. J. Fox, Gaussian 16 Revision B.01, Gaussian Inc., Wallingford CT 2016.
[61] T. M. Henderson, A. F. Izmaylov, G. Scalmani, and G. E. Scuseria, J. Chem. Phys. **131**, 044108 (2009).
[62] F. Santoro, A. Lami, R. Improta, J. Bloino, and V. Barone, J. Chem. Phys. **128**, 224311 (2008).
[63] T. Bally, C. Carra, M. P. Fülscher, and Z. Zhu, J. Chem. Soc., Perk. Trans. 2 **8**, 1759 (1998).
[64] V. Blanchet, K. Raffael, G. Turri, B. Chatel, B. Girard, I. A. Garcia, I. Wilkinson, and B. J. Whitaker, J. Chem. Phys. **128**, 164318 (2008).
[65] M. H. Stockett, J. N. Bull, J. T. Buntine, E. Carrascosa, E. K. Anderson, M. Gatchell, M. Kaminska, R. F. Nascimento, H. Cederquist, H. T. Schmidt, and H. Zettergren, Eur. Phys. J. D **74**, 150 (2020).
[66] B. Zhu, J. N. Bull, M. Ji, H. Zettergren, and M. H. Stockett, J. Chem. Phys. **157**, 044303 (2022).
[67] K. Hansen, J. U. Andersen, P. Hvelplund, S. P. Møller, U. V. Pedersen, and V. V. Petrunin, Phys. Rev. Lett. **87**, 123401 (2001).
[68] J. U. Andersen, E. Bonderup, and K. Hansen, J. Chem. Phys. **114**, 6518 (2001).
[69] S. Martin, J. Bernard, R. Brédy, B. Concina, C. Joblin, M. Ji, C. Ortega, and L. Chen, Phys. Rev. Lett. **110**, 063003 (2013).
[70] S. Martin, M. Ji, J. Bernard, R. Brédy, B. Concina, A. R. Allouche, C. Joblin, C. Ortega, G. Montagne, A. Cassimi, Y. Ngono-Ravache, and L. Chen, Phys. Rev. A **92**, 053425 (2015).
[71] J. Becker, C. Wentrup, E. Katz, and K. P. Zeller, J. Am. Chem. Soc. **102**, 5110 (1980).
[72] M. J. S. Dewar and K. M. Merz, J. Am. Chem. Soc. **108**, 5142 (1986).
[73] L. T. Scott and G. K. Agopian, J. Am. Chem. Soc. **99**, 4506 (1977).
[74] L. J. Allamandola, A. G. G. M. Tielens, and J. R. Barker, Astrophys. J. **290**, L25 (1985).
[75] L. J. Allamandola, G. G. M. Tielens, and J. R. Barker, Astrophys. J. Supp. Ser. **71**, 733 (1989).
[76] C. Joblin and A. G. G. M. Tielens, *PAHs and the Universe* (EDP Sciences, 2020).
[77] E. Peeters, S. Hony, C. V. Kerckhoven, A. G. G. M. Tielens, L. J. Allamandola, D. M. Hudgins, and C. W. Bauschlicher, Astron. Astrophys. **390**, 1089 (2002).
[78] H. Andrews, C. Boersma, M. W. Werner, J. Livingston, L. J. Allamandola, and A. G. G. M. Tielens, Astrophys. J. **807**, 99 (2015).
[79] M. J. F. Rosenberg, O. Berné, and C. Boersma, Astron. Astrophys. **566**, L4 (2014).
[80] E. Peeters, H. W. W. Spoon, and A. G. G. M. Tielens, Astrophys. J. **613**, 986 (2004).
[81] O. Berné, C. Joblin, A. Fuente, and F. Ménard, Astron. Astrophys. **495**, 827 (2009).
[82] M. C. R. Cockett, H. Ozeki, K. Okuyama, and K. Kimura, J. Chem. Phys. **98**, 7763 (1993).
[83] B. J. West, L. Lesniak, and P. M. Mayer, J. Phys. Chem. A **123**, 3569 (2019).
[84] A. Simon and M. Rapacioli, in *Chemical Modelling* (Royal Society of Chemistry) pp. 195–216.
[85] U. R. Kadhane, M. V. Vinitha, K. Ramanathan, A. S., J. Bouwman, L. Avaldi, P. Bolognesi, and R. Richter, J. Chem. Phys.

156, 244304 (2022).
[86]K. Ramanathan, A. S., J. Bouwman, L. Avaldi, M. V. Vinitha, P. Bolognesi, R. Richter, and U. R. Kadhane, J. Chem. Phys. **157**, 064303 (2022).
[87]Y. Ling and C. Lifshitz, J. Phys. Chem. A **102**, 708 (1998).
[88]H. A. B. Johansson, H. Zettergren, A. I. S. Holm, N. Haag, S. B. Nielsen, J. A. Wyer, M.-B. S. Kirketerp, K. Støchkel, P. Hvelplund, H. T. Schmidt, and H. Cederquist, J. Chem. Phys. **135**, 084304 (2011).
[89]S. Banhatti, D. B. Rap, A. Simon, H. Leboucher, G. Wenzel, C. Joblin, B. Redlich, S. Schlemmer, and S. Brünken, Phys. Chem. Chem. Phys. **24**, 27343 (2022).
[90]A. Simon, M. Rapacioli, G. Rouaut, G. Trinquier, and F. X. Gadéa, Philos. Trans. R. Soc. A **375**, 20160195 (2017).
[91]T. Chen, Y. Luo, and A. Li, Astron. Astrophys. **633**, A103 (2020).